Reconciling LED and monochromator-based measurements of spectral responsivity in solar cells

John Roller and Behrang H. Hamadani*

Engineering Laboratory, National Institute of Standards and Technology, Gaithersburg, MD 20899, USA
**behrang.hamadani@nist.gov*

Abstract: The irradiance spectral responsivity is an important measurement characteristic for a solar cell and has served as a primary reference cell calibration parameter for a growing number of national laboratories in recent years. This paper discusses the process by which a packaged reference cell is calibrated using the power spectral responsivity from a monochromator-based measurement coupled with discrete irradiance responsivity measurements from a light emitting diode (LED) array source to uniformly illuminate the cell. To accurately transfer the responsivity from a calibrated detector cell to a fully packaged reference cell, differences in the measurements of power and irradiance responsivities due to the two separate lighting sources must be reconciled. The spectral effects of using LEDs, as well as other physical packaging effects, are discussed in detail and a comprehensive treatment of the uncertainty components from both approaches is presented.

1. Introduction

The spectral responsivity [1–5] of a photovoltaic (PV) solar cell, R, can be measured and quantified in two ways. One is the power spectral responsivity (R_{pwr}) which captures the spectral dependence of the cell's short circuit current (I_{sc}) when normalized by the incident radiant power of the monochromatic beam. The other is the irradiance spectral responsivity (R_{irr}) which describes the behavior of I_{sc} normalized by the input irradiance over the spectral region of response. Power spectral responsivity measurements are generally performed with a beam diameter smaller than the active device area, therefore underfilling the device. For absolute measurements, the beam power is determined by using a reference photodetector that has also been previously calibrated under an underfilling beam, preferably by an accredited national laboratory [6]. For the irradiance spectral responsivity measurements, the irradiance or incident power per unit area of the monochromatic beam is required. Irradiance can be determined by fully illuminating (i.e., overfilling) a uniform, apertured photodetector with collimated and uniform monochromatic radiation and then dividing the measured beam power by the aperture area. The power spectral responsivity has SI units of A W^{-1}, whereas the irradiance spectral responsivity is reported in units of A m^2 W^{-1}.

Irradiance spectral responsivity measurements are generally difficult to perform because the experimenter needs to produce a very uniform (spatial power variations under 2 %), stable, overfilling, and spectrally tunable and collimated beam that can be measured accurately. For these reasons, most experimental setups are based on power responsivity and are used to report the external quantum efficiency (EQE) of the device under test (DUT), typically as a normalized measurement. However, there is a very compelling reason to pursue irradiance spectral responsivity measurements: determination of the I_{sc} under a given illumination condition, in particular the standard reporting conditions (SRC) with the air mass 1.5 global (AM 1.5 G) spectrum. In fact, this method has been employed by various national metrology laboratories for reference solar cell calibrations [7–9] with total expanded uncertainties of one percent or less for the I_{sc} calculation. This approach has been so successful that it is quickly becoming the method of choice for primary calibration of reference solar cells. Designing an irradiance spectral response system centered on a monochromator with traditional light sources such as xenon or halogen lamps has been achieved with reasonably good results [7,9], although the output light intensity and uniformity is always a challenge and more complex systems utilizing tunable lasers have been deployed to overcome some of these challenges [10].

Single color light emitting diodes (LEDs) have also been used as bright and uniform light sources to perform spectral responsivity measurements, although bandwidths greater than 15 nm, asymmetric emission profiles, and the limited choices of emission wavelengths introduce uncertainty in characterizing the response for a specific wavelength. In some cases, only LEDs with bandwidths less than 40 nm were deployed in order to minimize the effect of the spectral profile on the measurement [11], while others have included a calibration factor to compensate for the broad spectral profile calculated through fourth-order polynomial modeling [12] or used the sum of several gaussian curves to reduce the mismatch between the modeled and measured LED spectrum [13]. Another approach used the LED spectra to form a set of orthonormal basis functions to reconstruct the spectral responsivity curves, but this can result in oscillatory behavior that must be corrected with a correction factor [14]. For these reasons, our group has focused our efforts on hybrid measurements, i.e., complementing LED-based measurements with monochromator-based measurements, particularly when designing and calibrating World Photovoltaic Scale (WPVS)-packaged reference solar cells or when the irradiance spectral responsivity of a given cell is needed.

In a previous work, we described a hybrid monochromator/LED based approach that would allow determination of the irradiance spectral response curve of an entire solar cell by first obtaining the power spectral responsivity data from the monochromator system and then scaling those data by a single or multi-LED-point scaling factor [1]. In a subsequent work, we expanded the LED system to a setup consisting of an LED array with a wide range of wavelengths coupled into an integrating sphere for better light uniformity. This system projected light over a large area and was fully automated to perform discrete irradiance spectral responsivity measurements [15,16]. However, outstanding issues regarding the LED emission profiles, discreteness of the data, overfill vs. underfill issues, uncertainty of the LED scaling factors, and the propagation of uncertainties for the constructed whole-cell irradiance spectral responsivity curve were mostly neglected. In this work, we outline a detailed mathematical approach that allows for reconciliation of the two measurement approaches and properly propagates all the major components of uncertainty for both setups to the final calculation of the I_{sc} under the standard reporting conditions. This approach also allows for small corrections to the R_{pwr} curves in the cases where R_{irr} LED measurements show some overfill effects related to the packaging of the solar cell.

2. Experimental setup and calibration

2.1 Measurement setup

The monochromator-based system, a differential spectral responsivity system (DSR), has been discussed in detail elsewhere [1] and consists of a dual light source: A 150 W Xe light source and a 100 W quartz tungsten halogen (QTH) light source. The former is used for the spectral range of 300 nm to 600 nm and the latter is used for the spectral range above 600 nm. The broadband light from these sources passes through order-sorting filters and a mechanical chopper for light modulation. The modulated monochromatic light that exits the monochromator illuminates the sample at a local spot and induces the cell to output an alternating current that is detected by a lock-in amplifier via a custom-designed transimpedance preamplifier. A DC operated LED-array of 8 high power LEDs with wavelengths ranging from 460 nm to 940 nm simultaneously illuminates the cell to provide light bias and push the cell to operate in the linear regime [17]. A small portion of the monochromator's light output is directed towards a sandwiched Si/Ge monitor detector, whose response is measured by a second transimpedance/lock-in amplifier. The signal is used to determine the radiant power of the monochromatic beam. A calibrated UV-enhanced silicon reference detector was used to calibrate the sandwiched Si/Ge monitor detector from 280 nm to 300 nm and a second calibrated Si reference detector covered the range 300 nm to 1100 nm. A calibrated Ge detector was used to calibrate the 1100 nm to 1800 nm range. Measurements were taken every 5 nm for the first detector and every 10 nm for the other two detectors. It is noted that for all silicon cell measurements in this paper, all 3 calibrated detectors are utilized, while for the GaAs cell, only the first two reference detectors are used.

For the discrete R_{irr} measurements, a custom-designed system based on an LED array coupled to a 50.8 cm integrating sphere was realized [15]. Briefly, the system consists of an LED-array plate with 32 LEDs ranging in center wavelength from 373 nm to 1193 nm, an output port with a diameter of 22.9 cm that projects light onto a sample stage, and two 1.3 cm ports that accommodate the attachment of one Si monitor detector and one Ge monitor detector to determine the irradiance of the powered LED. A central baffle built into the sphere promotes uniform light output. Each of the LEDs that are mounted on a water-cooled heat sink is sequentially pulsed by an LED driver at a user specified frequency (1 Hz to 5 kHz) and current. The AC photocurrent signal from both the test cell and the monitor detector is amplified and measured by current preamplifiers and a lock-in amplifier. The irradiance scale is transferred onto the sphere system by first determining an effective area for the reference Si detector with calibrated power responsivity. This effective area, which has a slight wavelength dependence, is found via a direct substitution measurement against an area-calibrated aperture mounted in front of the detector. A calibration procedure is then used where this reference detector is mounted at the location of the test plane and its irradiance spectral responsivity scale is transferred onto the monitor detectors. To calibrate the monitor detectors, only the Si calibration detector for wavelengths between 300 nm and 1100 nm was used. Measurements were taken with each of the 32 LEDs within that wavelength range.

2.2 Calibration procedure

To calibrate the instruments that are used for measuring the responsivity, measurements on NIST-calibrated reference detectors are taken on both setups. This process calibrates the built-in monitor detectors for measurements of the input radiant power (or input irradiance) on test cells. This input power (or irradiance) can be calculated by measuring the output voltages of both the monitor detector, V_{m}, and the calibrated reference detector, V_{s}, through the lock-in measurements on both apparatuses. Both the monitor and the reference detectors are measured in volts (RMS) because their output signals run through transimpedance amplifiers with gain, G. The current from each detector can therefore be represented as $V_{\mathrm{m}}/G_{\mathrm{m}}$ and $V_{\mathrm{s}}/G_{\mathrm{s}}$ for the monitor and reference detectors, respectively. Since the detector responsivity, $R_{\mathrm{s}}(\lambda)$, is a known and calibrated set of values, the responsivity of the monitor detector can be calculated using the input power (or irradiance) with the equations

$$P_{in} = \frac{V_{\mathrm{s}} / G_{\mathrm{s}}}{R_{\mathrm{s}}(\lambda)} = \frac{V_{\mathrm{m}} / G_{\mathrm{m}}}{R_{\mathrm{m}}(\lambda)}\,, \tag{1}$$

for the monochromator and

$$E_{e,in} = \frac{V_{\mathrm{s}}^{*} / G_{\mathrm{s}}}{R_{\mathrm{s,\,LED}}^{*} A_{\mathrm{s}}} = \frac{V_{\mathrm{m}}^{*} / G_{\mathrm{m}}}{R_{\mathrm{m,LED}}^{*} A_{\mathrm{m}}}\,, \tag{2}$$

for the integrating sphere LED setup where the detectors have *effective active* area, A, and the responsivity of a detector to an LED, R^{*}, is given as a function of the LED emission profile, E_{LED}, as measured in terms of spectral irradiance at the measurement plane by a calibrated spectroradiometer:

$$R_{LED}^{*} = \frac{\int_{\lambda_{\min}}^{\lambda_{\max}} R(\lambda) E_{\mathrm{LED}}(\lambda) \mathrm{d}\lambda}{\int_{\lambda_{\min}}^{\lambda_{\max}} E_{\mathrm{LED}}(\lambda) \mathrm{d}\lambda} . \quad (3)$$

The normalized LED outputs that are the foundation for using the term R^* can be seen in Fig. 1. The spectroradiometer consists of two separate detectors, an ultraviolet-visible (UV-Vis) detector with spectral range 250 nm to 1024 nm and a near infrared (NIR) detector with range 940 nm to 1698 nm, each detector calibrated against an FEL lamp.

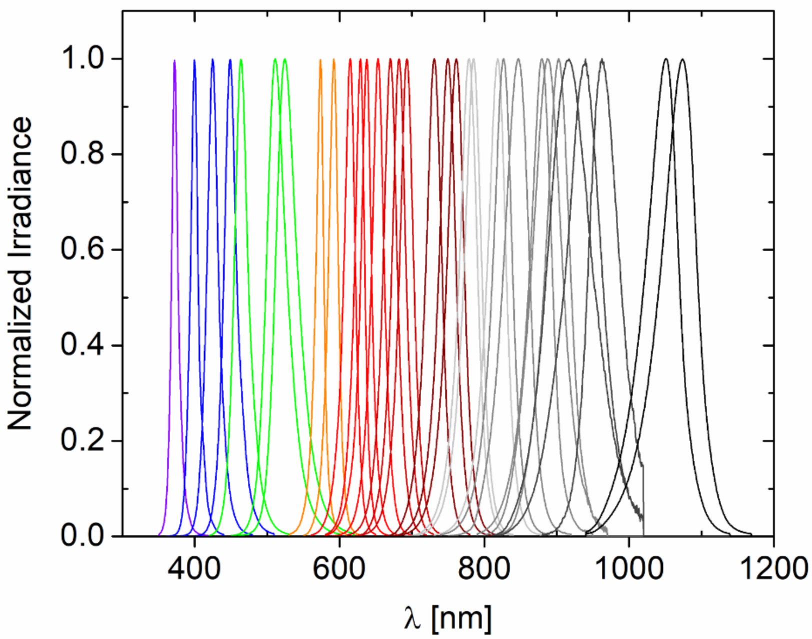

Fig. 1. Normalized irradiance profiles for the 32 LEDs used in the integrating sphere system. The truncated tail of the LED with center wavelength at 966.7 nm is due to the range limit of the UV-Vis detector.

For the calculations of the area of the calibrated reference detector, A_s, the whole of the reference diode area is used as opposed to an apertured portion of it. This area is used because the device is a packaged diode with a glass cover and a mounted aperture on glass a few mm from the diode surface may not correctly represent the actual illumination area when exposed to diffuse or partly collimated light. To determine A_s, we first place a calibrated pinhole aperture of area A_{ap} at the center of the reference detector which is very uniform (typically to within 0.1 %). The reference detector is then measured with and without the aperture and the total area is calculated using Equation 4:

$$A_{\mathrm{s,LED}} = \frac{V_{\mathrm{s}}^{*} / G_{\mathrm{s}}}{R_{\mathrm{s,LED}}^{*}} \cdot \frac{1}{V_{\mathrm{m,s}}^{*} / G_{\mathrm{m,s}}} \cdot \frac{R_{\mathrm{ap,LED}}^{*} A_{\mathrm{ap}}}{V_{\mathrm{ap}}^{*} / G_{\mathrm{ap}}} \cdot V_{\mathrm{m,ap}}^{*} / G_{\mathrm{m,ap}} . \quad (4)$$

For this area calibration process, the measurement plane is at a distance of 125 cm from the integrating sphere as to verify that the light incident on the aperture is mostly collimated. $V_{\mathrm{m,s}}^{*}$ and $V_{\mathrm{m,ap}}^{*}$ are the monitor voltages for the non-apertured and apertured measurements respectively. It should be noted that the resulted A_s is LED (wavelength) dependent because the uniformity of the diode near the edge pixels gets worse and will have a wavelength dependence. Even so, the majority of the calculated A_s values are within a tight bound of 1 %. Once A_s is determined, the detector is placed at the normal measurement plane much closer to the sphere for calibration of the monitor diodes and regular subsequent solar cell measurements.

3. Responsivity measurement procedure

3.1 Responsivity measurement

Test cell measurements can now be done on both the monochromator and the integrating sphere setups with the test cell replacing the calibrated reference detector. This replacement results in similar equations:

$$P_{in} = \frac{V_{\mathrm{t}} / G_{\mathrm{t}}}{R_{\mathrm{t}}(\lambda)} = \frac{V_{\mathrm{m}} / G_{\mathrm{m}}}{R_{\mathrm{m}}(\lambda)} \tag{5}$$

for the monochromator and

$$E_{e,in} = \frac{V_{\mathrm{t}}^{*} / G_{\mathrm{t}}}{R_{\mathrm{t,LED}}^{*} A_{\mathrm{t}}} = \frac{V_{\mathrm{m}}^{*} / G_{\mathrm{m}}}{R_{\mathrm{m,LED}}^{*} A_{\mathrm{m}}} \tag{6}$$

for the integrating sphere, where the subscript t refers to the test cell. Notice that A_{t} and A_{m} represent an effective area for both the test device and the monitor detector that result in a photocurrent signal generated by the device. In other words, dead detector regions, metalized fingers, or bus bars on the cell are excluded from this defined area. Since the signal input may change between measurements, the input power between the reference and test cell measurements may change. This variation will cause the voltages to fluctuate, but the responsivities and areas will remain constant throughout the measurement. The measurement equations for the responsivity calculations are shown in Equations 7 and 8, where the subscript 1 refers to the reference measurement (for calibration of the monitor detector) and 2 refers to the test measurement:

$$R_{\mathrm{t,Mono}}(\lambda) = V_{\mathrm{t}} / G_{\mathrm{t}} \cdot \frac{R_{\mathrm{m}}(\lambda)}{V_{\mathrm{m2}} / G_{\mathrm{m2}}} = V_{\mathrm{t}} / G_{\mathrm{t}} \cdot \frac{1}{V_{\mathrm{m2}} / G_{\mathrm{m2}}} \cdot \frac{R_{\mathrm{s}}(\lambda)}{V_{\mathrm{s}} / G_{\mathrm{s}}} \cdot V_{\mathrm{m1}} / G_{\mathrm{m1}}, \tag{7}$$

$$R_{\mathrm{t,LED}}^{*} A_{\mathrm{t}} = V_{\mathrm{t}}^{*} / G_{\mathrm{t}} \cdot \frac{1}{V_{\mathrm{m2}}^{*} / G_{\mathrm{m2}}} \cdot \frac{R_{\mathrm{s}}^{*} A_{\mathrm{s}}}{V_{\mathrm{s}}^{*} / G_{\mathrm{s}}} \cdot V_{\mathrm{m1}}^{*} / G_{\mathrm{m1}}. \tag{8}$$

A silicon test cell was first measured with the monochromator from 280 nm to 1200 nm at intervals of 10 nm. The cell was then measured with the integrating sphere for each of the 32 LEDs. The responsivities of these two measurements were then calculated using Equations 7 and 8 and can be seen in Fig. 2 for a typical packaged silicon solar cell.

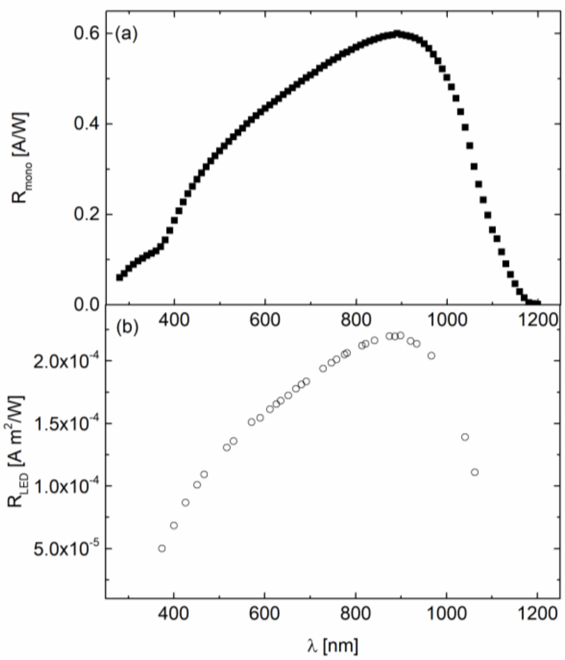

Fig. 2. Responsivity measurements from the monochromator (a) and the integrating sphere (b) of a WPVS-packaged silicon solar cell. Note that the monochromator measurement is a power responsivity, and the integrating sphere is an irradiance responsivity. For the integrating sphere measurement, responsivities are plotted at the LED center wavelength.

The integrating sphere responsivity output is not simply a scalar multiple of the monochromator responsivity curve. Since the LEDs are outputting light at a broader spectrum than the monochromator, the responsivity measured with the integrating sphere is a weighted average of the responsivities in the broad output wavelength spectrum of the LED.

3.2 Combining measurements

Once these two sets of measurements of spectral responsivity data have been determined, an appropriate scaling factor (SF) needs to be calculated to construct the whole-cell irradiance spectral response curve. To calculate the proper wavelength-dependent area scaling factor for each power responsivity (monochromator) data point, a scaling factor is first calculated for each integrating sphere LED, given by

$$SF_{LED} = \frac{R^*_{\mathrm{t,LED}} A_{\mathrm{t}}}{R^*_{\mathrm{t,Mono}}} \ . \tag{9}$$

As the monochromator measurement provides a calculation of the power responsivity, $R_{\mathrm{t}}(\lambda)$, and the LED emission spectra are also measured, an effective power responsivity, $R^*_{\mathrm{t,Mono}}$, is calculated for each LED so each integrating sphere measurement can be compared to the monochromator measurements according to

$$R^*_{\mathrm{t,Mono}} = \frac{\int_{\lambda_{\min}}^{\lambda_{\max}} R_{\mathrm{t,Mono}}(\lambda) E_{\mathrm{LED}}(\lambda) \mathrm{d}\lambda}{\int_{\lambda_{\min}}^{\lambda_{\max}} E_{\mathrm{LED}}(\lambda) \mathrm{d}\lambda} \ . \tag{10}$$

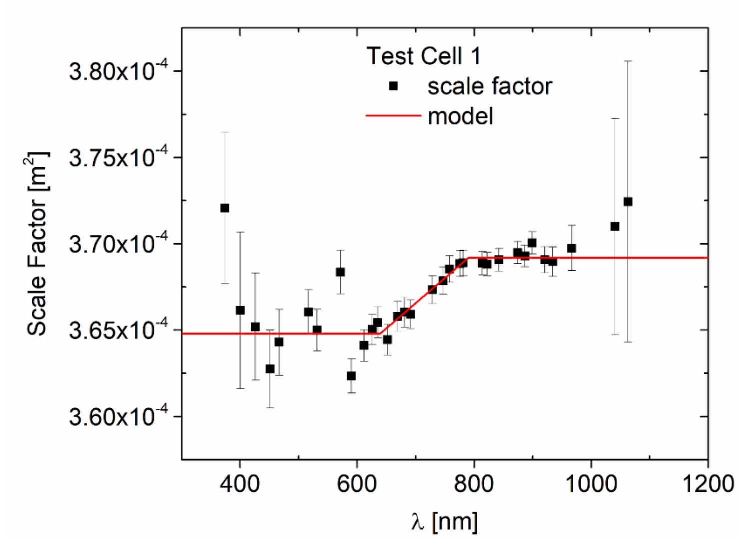

Fig. 3. A piecewise linear model is fitted to the calculated scaling factors for the silicon test cell using the uncertainty of the scaling factor in the weighting function. The packaging changes the effective area for higher wavelengths of incident light.

$R_{t,Mono}(\lambda)$ is a first order interpolation of the monochromator power responsivity data. Under ideal circumstances where the test cell is comprised of a uniform material and the shape of the monochromator spectral responsivity curve is beam-position independent and representative of the entire cell, SF values calculated by Equation 9 are wavelength-independent and can be represented by a single SF. However, sometimes the monochromator and LED measurements show responsivity curves that are slightly different in shape, resulting in scaling factors that have a wavelength dependence. One reason for this effect is related to the packaging of the solar cell. The monochromator measurement is an underfill measurement whereas the LED measurement fully overfills the cell and the packaging material around the mounted cell. The anodized aluminum surface of the cell holder, particularly in the immediate area around the mounted solar cell, starts to show increased reflection at wavelengths above 700 nm. This increased reflection can lead to secondary reflections at the backside of the glass cover and eventually couple into the active region in the center of the cell. Reflections in the packaging cause an increased irradiance responsivity in the higher wavelength region. An overfill measurement is the appropriate type of measurement for irradiance responsivity, R_{irr}, and short circuit current, I_{sc}, calculations since reference cells are generally also fully illuminated under a solar simulator or outdoors under the sun. This effect was verified by a pair of measurements where a cell was measured at each LED with (a) only the packaging and (b) with a square shaped aperture to allow only direct light to reach the cell. The ratio of these two measurements showed the same shape as the scaling factors when plotted as a function of wavelength.

The results for the SF calculation for the silicon test cell are plotted in Fig. 3 along with the total standard uncertainty (k=1) plotted as an error bar for each point (details on the uncertainty calculation can be seen in the Uncertainty Analysis section). As described previously, the step that appears in the SF data at $\lambda \approx 700$ nm is due to the reflections in the cell packaging and has been observed and verified in other cell holder packages. To account for this issue, a scalar model is developed with four degrees of freedom consisting of two constant segments on either side of the step and a linear segment in the middle that connects the two constant segments as is shown in Fig. 3. A constant was chosen in the longer wavelength region because the cell was previously measured to have good uniformity and the high uncertainty on the two last points made those points insufficient to justify a linear fit.

To build the wavelength-dependent SF model, (*Assumption 1*) each LED was assumed to be representative of its center wavelength, λ_c as calculated by:

$$\lambda_{c,\mathrm{LED}} = \frac{\int_{\lambda_{\min}}^{\lambda_{\max}} \lambda E_{\mathrm{LED}}(\lambda)\mathrm{d}\lambda}{\int_{\lambda_{\min}}^{\lambda_{\max}} E_{\mathrm{LED}}(\lambda)\mathrm{d}\lambda} \quad . \tag{11}$$

The LEDs were grouped into three different sets (short, middle, and long wavelengths), and a linear fit was calculated using a weighted least sum of squares method. The weights for each point were given as one over the uncertainty of the scaling factor squared,

$$w_{LED} = \frac{1}{U_{SF,LED}{}^{2}} , \tag{12}$$

and the linear model was calculated such that, for each LED, i, it minimized the sum

$$\sum_{i=1}^{\mathrm{LEDs}} w_i \left(SF\mathrm{model}(\lambda_{c,i}) - SF_i \right)^2 . \tag{13}$$

The calculation of the SF uncertainty is detailed in the Uncertainty Analysis section. The overall irradiance responsivity, $R_{\mathrm{t,irr}}$ of the cell can now be calculated using the power responsivity (monochromator) data and the area scaling factor calculated in the previous step:

$$R_{\mathrm{t,irr}}(\lambda) = R_{\mathrm{t,Mono}}(\lambda) SF\mathrm{model}(\lambda) . \tag{14}$$

4. Uncertainty analysis

In addition to providing the overall uncertainty to the responsivity measurement, the uncertainty must be propagated through the calculations to use in weighting terms for the scaling factor calculation. To begin the uncertainty calculation process, we first look at the uncertainty of the individual measurements.

To calculate the uncertainty of the power responsivity, R_t, generated from the monochromator, the uncertainties of the measured components are combined. One of the largest sources of uncertainty is related to the reference detector calibrations U_{Rs} which is provided with the NIST calibrated reference detector. Each voltage value is measured N times (with N = 50, typically) at each wavelength to find the mean and the standard deviations of the fluctuations caused by various sources of noise in the system. For the uncertainty of the electrical current values (voltages over transimpedance gains), the standard deviation was calculated using the N measurements of V/G. The uncertainty of the mean value was then obtained using the relationship for a normal distribution of values:

$$U_{V/G} = \frac{\sigma_{V/G}}{\sqrt{N}} . \tag{15}$$

Only the standard deviation of the measurement was used for this uncertainty because other sources of error, namely the type B uncertainties from the sensitivity settings of the lock-in amplifier and the gain setting of the transimpedance amplifier, were investigated in detail and found to be insignificant by comparison to the standard deviation.

Another important source of uncertainty is the sensitivity to errors in the input wavelength, $\partial R_t / \partial \lambda$. To calculate this value, an interpolation of the data is taken with respect to the incident wavelength, λ. To create this interpolation, all data points for $R_t(\lambda)$ are given by Equation 7 above. A first order interpolation is then performed that allows for the calculation of the sensitivity of R_t to wavelength at each specified wavelength. The uncertainty from the incident wavelength, $U_{R_{\mathrm{t},\lambda}}$, is then given as the product of the sensitivity of R_t and a given uncertainty in wavelength, U_λ :

$$U_{R_{\mathrm{t},\lambda}} = \frac{\partial R_\mathrm{t}(\lambda)}{\partial \lambda} U_\lambda \,. \tag{16}$$

The value of U_λ is estimated to be 0.5 nm based on the wavelength calibration of the monochromator using pen lights or laser lines with tabulated emission characteristics. Finally, there is a spectral-independent, relative reproducibility uncertainty component, $U_{\mathrm{rep,rel}}$ estimated to be 0.11 % for the silicon reference detector (300 nm to 1100 nm calibration range) and as high as 0.7 % for the germanium reference detector (1110 nm to 1900 nm). This component represents the combined repeatability and reproducibility of the calibration of the monitor detectors against the reference detector. This Type B uncertainty was determined by conducting calibration measurements over several days for each detector and determining the standard deviation of all measurements.

Combining all uncertainty components, the uncertainty on the power responsivity for the monochromator is given by

$$U_{R_{\mathrm{t,Mono}}} = \begin{pmatrix} \left(\frac{U_{R_\mathrm{s}}}{R_\mathrm{s}}\right)^2 + \left(\frac{U_{V_\mathrm{t}/G_\mathrm{t}}}{V_\mathrm{t}/G_\mathrm{t}}\right)^2 + \left(\frac{U_{V_\mathrm{s}/G_\mathrm{s}}}{V_\mathrm{s}/G_\mathrm{s}}\right)^2 + \left(\frac{U_{V_\mathrm{m1}/G_\mathrm{m1}}}{V_\mathrm{m1}/G_\mathrm{m1}}\right)^2 + \left(\frac{U_{V_\mathrm{m2}/G_\mathrm{m2}}}{V_\mathrm{m2}/G_\mathrm{m2}}\right)^2 + \\ \left(\frac{U_{R_{\mathrm{t},\lambda}}}{R_\mathrm{t}}\right)^2 + \left(\frac{U_{\mathrm{rep,rel}}}{100}\right)^2 \end{pmatrix}^{1/2} R_\mathrm{t} \,. \tag{17}$$

The uncertainty of the irradiance responsivity, $R_\mathrm{t}^* A_\mathrm{t}$, generated from the integrating sphere LED source is calculated in a similar manner as that for the power responsivity, R_t. Each of the electrical current values (voltages over transimpedance gains) have an uncertainty based on the standard deviation of N measurements as given by Equation 15. In addition, the reference detector uncertainty, $U_{R_\mathrm{s}^*}$, is calculated using an interpolation on the given reference detector uncertainty data:

$$U_{R^*_{\mathrm{s,LED}}} = \frac{\int_{\lambda_{\min}}^{\lambda_{\max}} U_{R_\mathrm{s}}(\lambda) E_{\mathrm{LED}}(\lambda) \mathrm{d}\lambda}{\int_{\lambda_{\min}}^{\lambda_{\max}} E_{\mathrm{LED}}(\lambda) \mathrm{d}\lambda} \,. \tag{18}$$

Note that for the above calculation, only relative LED irradiance values are needed and the equation above represents an upper limit for $U_{R^*_{\mathrm{s,LED}}}$ [18]. The E_{LED} is treated without considering its uncertainty or its propagation because the spectroradiometer is calibrated against a stable light source and the relative shape of the LED emission profile is accurate. The area uncertainty for the reference detector measurement, U_{A_s} is calculated using the uncertainties of the several measurements used in Equation 4:

$$U_{A_\mathrm{s}} = \begin{pmatrix} \left(\frac{U_{R_\mathrm{s}^*}}{R_\mathrm{s}^*}\right)^2 + \left(\frac{U_{V_\mathrm{s}^*/G_\mathrm{s}}}{V_\mathrm{s}^*/G_\mathrm{s}}\right)^2 + \left(\frac{U_{V^*_\mathrm{m,s}/G_\mathrm{m,s}}}{V^*_\mathrm{m,s}/G_\mathrm{m,s}}\right)^2 + \left(\frac{U_{R^*_\mathrm{ap}}}{R^*_\mathrm{ap}}\right)^2 + \left(\frac{U_{A_\mathrm{ap}}}{A_\mathrm{ap}}\right)^2 + \\ \left(\frac{U_{V^*_\mathrm{ap}/G_\mathrm{ap}}}{V^*_\mathrm{ap}/G_\mathrm{ap}}\right)^2 + \left(\frac{U_{V^*_\mathrm{m,ap}/G_\mathrm{m,ap}}}{V^*_\mathrm{m,ap}/G_\mathrm{m,ap}}\right)^2 \end{pmatrix}^{1/2} A_\mathrm{s} \,. \tag{19}$$

Since the LEDs are discrete light sources with different emission profiles and effective bandwidths, there is no direct and high-resolution measurement for $R_{\mathrm{t}}(\lambda)$. This lack of resolution means that an accurate calculation of $\partial R_{\mathrm{t}} / \partial\lambda$ is not possible. Therefore, a first order interpolation on the points $R^{*}_{\mathrm{t,LED}}$ at LED centroid wavelengths $\lambda_{\mathrm{c,LED}}$ is used as an approximation of $R_{\mathrm{t}}(\lambda)$.

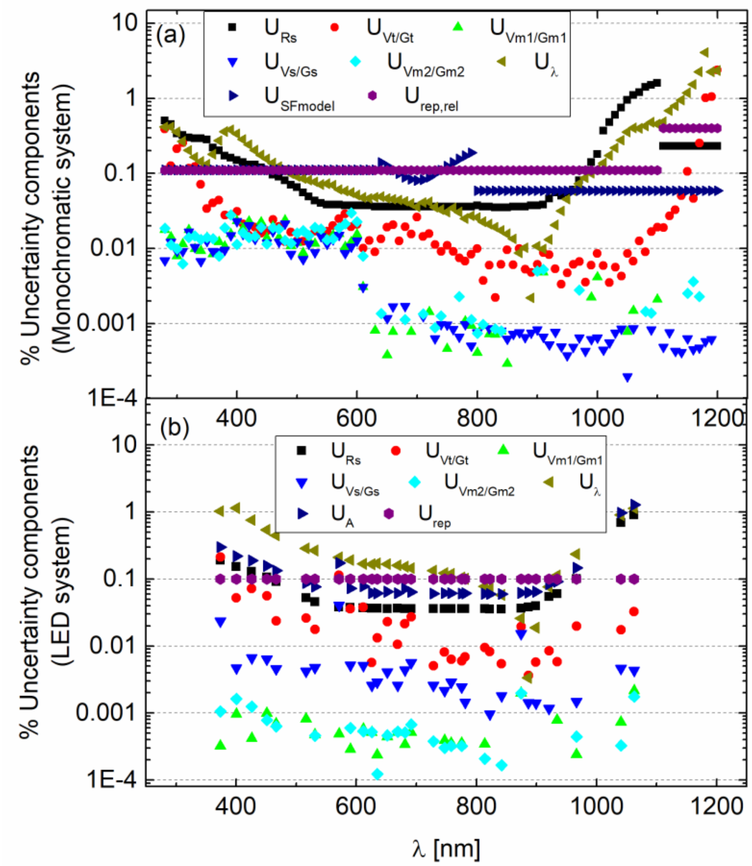

Fig. 4. Components of uncertainty calculation for the (a) monochromator and (b) integrating sphere (LED) systems.

The wavelength uncertainty calculated from the interpolation, $R^{*}_{\mathrm{t}}A_{\mathrm{t}}(\lambda)$, is assumed to be sufficiently close to the actual irradiance responsivity $R_{\mathrm{t,irr}}(\lambda)$. The validity of this assumption (*Assumption 2*) will be discussed in the verifying assumptions section and will be fixed if found incorrect. With this interpolation, the wavelength uncertainty is calculated by the equation:

$$U_{R^{*}_{\mathrm{t,irr},\lambda},LED} = \frac{\int_{\lambda_{\min}}^{\lambda_{\max}} \frac{\partial R_{\mathrm{t,irr}}(\lambda)}{\partial\lambda} U_{\lambda} E_{\mathrm{LED}}(\lambda)\mathrm{d}\lambda}{\int_{\lambda_{\min}}^{\lambda_{\max}} E_{\mathrm{LED}}(\lambda)\mathrm{d}\lambda} \approx \frac{\int_{\lambda_{\min}}^{\lambda_{\max}} \frac{\partial R^{*}_{\mathrm{t}}A_{\mathrm{t}}(\lambda)}{\partial\lambda} U_{\lambda} E_{\mathrm{LED}}(\lambda)\mathrm{d}\lambda}{\int_{\lambda_{\min}}^{\lambda_{\max}} E_{\mathrm{LED}}(\lambda)\mathrm{d}\lambda}. \quad (20)$$

The final uncertainties of the LED irradiance responsivity measurements are therefore given by:

$$U_{R^*_{\mathrm{t,LED}}A_{\mathrm{t}}} = \left(\left(\frac{U_{R^*_{\mathrm{s}}}}{R^*_{\mathrm{s}}}\right)^2 + \left(\frac{U_{A_{\mathrm{s}}}}{A_{\mathrm{s}}}\right)^2 + \left(\frac{U_{V^*_{\mathrm{t}}/G_{\mathrm{t}}}}{V^*_{\mathrm{t}}/G_{\mathrm{t}}}\right)^2 + \left(\frac{U_{V^*_{\mathrm{s}}/G_{\mathrm{s}}}}{V^*_{\mathrm{s}}/G_{\mathrm{s}}}\right)^2 + \left(\frac{U_{V^*_{\mathrm{m1}}/G_{\mathrm{m1}}}}{V^*_{\mathrm{m1}}/G_{\mathrm{m1}}}\right)^2 + \left(\frac{U_{V^*_{\mathrm{m2}}/G_{\mathrm{m2}}}}{V^*_{\mathrm{m2}}/G_{\mathrm{m2}}}\right)^2 + \left(\frac{U_{R^*_{\mathrm{t,irr},\lambda},LED}}{R^*_{\mathrm{t,LED}}A_{\mathrm{t}}}\right)^2 + \left(\frac{U_{\mathrm{rep,rel}}}{100}\right)^2 \right)^{1/2} R^*_{\mathrm{t,LED}}A_{\mathrm{t}} \,. \quad (21)$$

The various components of the uncertainty calculation for both responsivity measurement setups are shown in Fig. 4; the most dominant ones for the monochromator measurements are $U_{R\mathrm{s}}$, U_{rep}, and U_{λ} and for the integrating sphere system are $U_{R\mathrm{s}}$, $U_{A\mathrm{s}}$, U_{λ} and U_{rep}.
With the uncertainties of both the monochromator measured power responsivity and the LED measured irradiance responsivity now established, the uncertainties for the scaling factor calculation can now be determined. The uncertainty associated with each effective responsivity, $U_{R^*_{\mathrm{t,Mono}}}$, is calculated for each LED profile using the equation:

$$U_{R^*_{\mathrm{t,Mono}}} = \frac{\int_{\lambda_{\mathrm{min}}}^{\lambda_{\mathrm{max}}} U_{R_{\mathrm{t,Mono}}}(\lambda) E_{\mathrm{LED}}(\lambda)\mathrm{d}\lambda}{\int_{\lambda_{\mathrm{min}}}^{\lambda_{\mathrm{max}}} E_{\mathrm{LED}}(\lambda)\mathrm{d}\lambda} \,. \quad (22)$$

The uncertainty associated with each calculated scaling factor is then given as:

$$U_{\mathrm{SF,LED}} = \sqrt{\left(\frac{U_{R^*_{\mathrm{t,LED}}A_{\mathrm{t}}}}{R^*_{\mathrm{t,LED}}A_{\mathrm{t}}}\right)^2 + \left(\frac{U_{R^*_{\mathrm{t,Mono}}}}{R^*_{\mathrm{t,Mono}}}\right)^2}\, SF \,. \quad (23)$$

The uncertainty of the scaling factor model, $U_{SF\mathrm{model}}(\lambda)$, is then determined for each LED group. For any set of LED scaling factors fit to a single constant value, the uncertainties for all scaling factors in that set were calculated using the uncertainty on the weighted average expressed by:

$$U_{SF\mathrm{model}}(\lambda) = \sqrt{\frac{1}{\sum_{i=1}^{\mathrm{LEDs}} w_i}} \,, \quad (24)$$

using the weights calculated in Equation 12.

For every scaling factor set with a linear fit, the uncertainty was calculated at each wavelength using the uncertainty of a least squares fit. The uncertainty in the scaling factor at λ is calculated as the uncertainty of the least squares linear fit intercept when the data are shifted in the wavelength domain by an amount λ [18] and is given by:

$$U_{SF\mathrm{model}}(\lambda) = \sqrt{\frac{\sum_{i=1}^{\mathrm{LEDs}} w_i(\lambda_{\mathrm{c},i}-\lambda)^2}{\sum_{i=1}^{\mathrm{LEDs}} w_i \sum_{i=1}^{\mathrm{LEDs}} w_i(\lambda_{\mathrm{c},i}-\lambda)^2 - (\sum_{i=1}^{\mathrm{LEDs}} w_i(\lambda_{\mathrm{c},i}-\lambda))^2}} \,. \quad (25)$$

The U_{SFmodel}, plotted in Fig. 4a is used for determination of $U_{R_{\mathrm{t,irr}}}(\lambda)$ through Equation 26.

$$U_{R_{\mathrm{t,irr}}}(\lambda) = \sqrt{\left(U_{R_{\mathrm{t,Mono}}}(\lambda) SF\mathrm{model}(\lambda)\right)^2 + \left(U_{R_{\mathrm{t,Mono}}}(\lambda) U_{SF\mathrm{model}}(\lambda)\right)^2} \,. \quad (26)$$

5. Obtaining short circuit current

5.1 Verifying assumptions

Before the final calculation of the short circuit current, the assumptions made earlier need to be verified.

Assumption 1: LEDs are representative of their center wavelength for building the scaling factor model, $SF\text{model}(\lambda)$.

This can be verified if

$$SF\text{model}(\lambda_{\text{c}}) - \frac{\int_{\lambda_{\min}}^{\lambda_{\max}} SF\text{model}(\lambda) E_{\text{LED}}(\lambda)\text{d}\lambda}{\int_{\lambda_{\min}}^{\lambda_{\max}} E_{\text{LED}}(\lambda)\text{d}\lambda} \approx 0 . \qquad (27)$$

Equation 27 is calculated for each of the scaling factors and this verification is assumed to be valid if the difference is less than 0.02 % such that any error from this assumption will be insignificant by comparison to other errors.

Assumption 2: The interpolation $R_{\text{t}}^{*}A_{\text{t}}(\lambda)$ *made on the points* $(\lambda_{\text{c}}, R_{\text{t}}^{*}A_{\text{t}})$ *is sufficiently close to* $R_{\text{t,irr}}(\lambda)$ *for the calculation of* $U_{R_{\text{t}}^{*}A_{\text{t}},\text{LED}}$.

Now that $R_{\text{t,irr}}(\lambda)$ has been determined, the uncertainty from $U_{R_{\text{t,irr}},\lambda}$ is given as before:

$$U_{R_{\text{t,irr}},\lambda,LED} = \frac{\int_{\lambda_{\min}}^{\lambda_{\max}} \frac{\partial R_{\text{t,irr}}(\lambda)}{\partial \lambda} U_{\lambda} E_{\text{LED}}(\lambda)\text{d}\lambda}{\int_{\lambda_{\min}}^{\lambda_{\max}} E_{\text{LED}}(\lambda)\text{d}\lambda} . \qquad (28)$$

$U_{R_{\text{t}}^{*}A_{\text{t}},\text{LED}}$ can now be recalculated with the corrected wavelength uncertainty component. The original $U_{R_{\text{t}}^{*}A_{\text{t}},\text{LED}}$ is then compared with the recalculated version. If the difference between the new and the old values is greater than 0.01 %, then the analysis is redone using the new value for $U_{R_{\text{t}}^{*}A_{\text{t}},\text{LED}}$.

5.2 Short circuit calculation and uncertainty

After the assumptions have been verified, the short circuit current is calculated using the Air Mass 1.5 solar spectral irradiance spectrum, $AM15(\lambda)$.

$$I_{\text{sc}} = \int_{\lambda_{\min}}^{\lambda_{\max}} AM15(\lambda) R_{\text{t,irr}}(\lambda)\text{d}\lambda \ . \qquad (29)$$

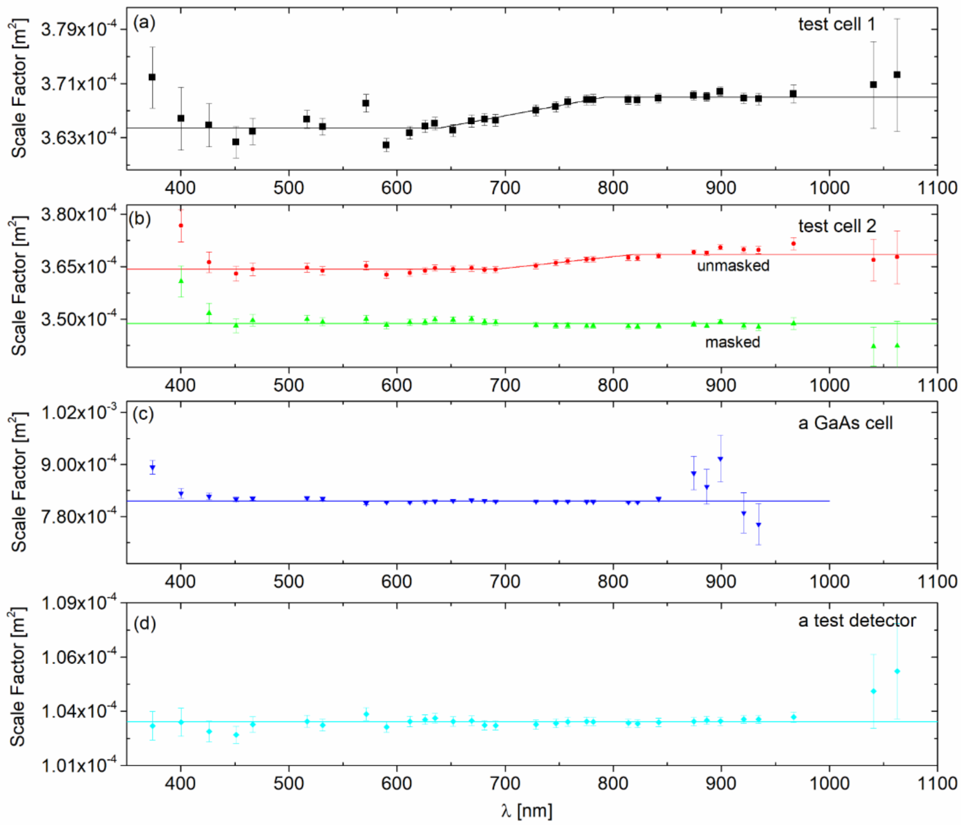

Fig. 5. A model is fit to the scaling factors calculated for all the measured samples. The primary silicon sample (a) is included for reference. A second silicon cell, masked and unmasked for package reflections (b), a gallium arsenide cell (c), and a silicon detector cell (d) are calculated with varying linear models.

It should be mentioned that $R_{\mathrm{t,irr}}(\lambda)$ must be obtained in the presence of an appropriate intensity of bias light so that the test cell operates in the linear regime. Due to the responsivity measurements being interdependent, an upper limit for uncertainty is calculated [18] and this limit will be the reported short circuit current uncertainty, $U_{I_{\mathrm{sc}}}$:

$$U_{I_{\mathrm{sc}}} = \int_{\lambda_{\min}}^{\lambda_{\max}} AM15(\lambda) U_{R_{\mathrm{t,irr}}}(\lambda) \mathrm{d}\lambda \,. \tag{30}$$

6. Results

Several other test cells were measured in a similar fashion to the first silicon cell. The calculation method is the same for all cells, except for the calculation of the area scaling factor. Fig. 5 shows the four area scaling factor models calculated for each of the cells. The second cell, silicon test cell 2, shows a behavior very similar to test cell 1, if measured as is (unmasked) and is modeled similar to test cell 1, with three line segments. However, if we mask the area on top of the glass corresponding to the black anodized packaging area around the cell (masked), the extra reflection effects from the packaging disappears and all the scaling factors can be modeled as one single line segment. The third cell shown is a gallium arsenide (GaAs) unpackaged cell. Due to the larger bandgap of the material, the cell is not responsive to all the

LEDs in the integrating sphere system. Of those LEDs used, a constant scaling factor is calculated. The last cell shown is a second silicon detector cell much like the one used as a reference detector for system calibration. This cell has a scaling factor model that is a single constant. This result arises because there is little packaging on the cell which removes the reflection effect, and the detector cell has good uniformity. The result of a constant scaling factor for the detector cell shows that the system has good transfer capability and is self-consistent.

With the area scaling factors now fully characterized and modeled, the final responsivity of each cell can be calculated as shown in Fig. 6. Note that while the responsivity curve for the GaAs cell is very different in shape from the silicon calibration detector, the spectral response is calculated with high accuracy. For silicon cells, we have generally observed that the irradiance responsivity uncertainty, $U_{R_{t,irr}}$, for a mid-wavelength value of 600 nm is about 0.17 % (k=1). Although the uncertainty increases to values above 1 % in the tail regions (λ > 1000 nm), its effects on the I_{sc} uncertainty are diminished in those regions. For example, for the silicon test cell 1 we measured I_{sc} = 125.13 ± 0.58 mA corresponding to a relative expanded uncertainty (k=2) of 0.46 %. For the silicon test cell 2, I_{sc} = 112.20 mA ± 0.5 mA is measured. For the GaAs cell, I_{sc} = 230.41 mA ± 1.06 mA is calculated.

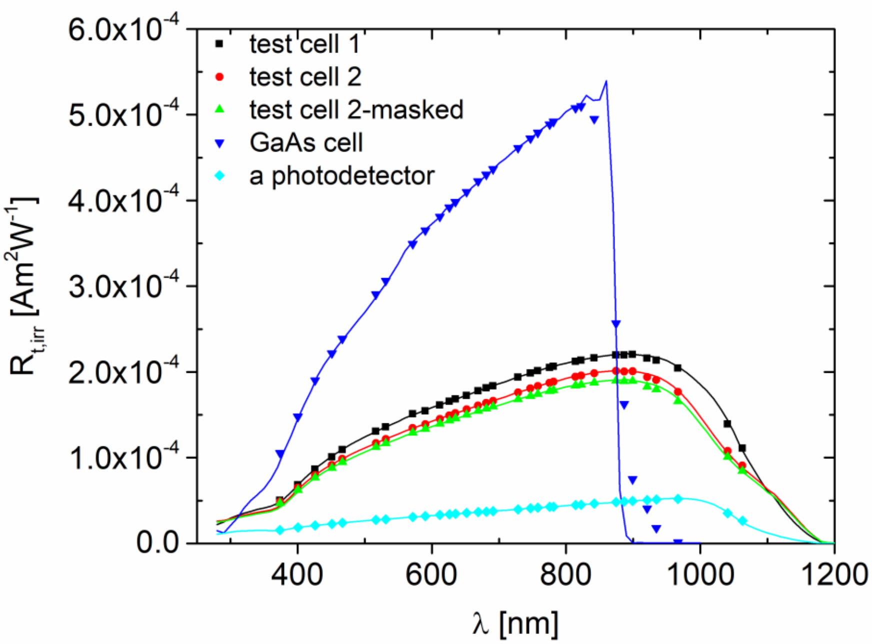

Fig. 6. Calculated responsivity curves (solid lines) for the measured cells. LED measurements (points) are included at their center wavelengths as a reference, but some do not line up with the final calculated responsivity due to spectral bandwidth effects.

7. Conclusions

The irradiance responsivity curve for a test cell in the overfill condition has been calculated through a combination of monochromator and LED measurements. The spectral effects of the LED bandwidth have been compensated for using the monochromatic data, and an appropriate area scaling factor has been calculated. This scaling factor also serves to reconcile the two measurement by creating a common parameter that links the two. The appropriate scaling factor was shown to be wavelength dependent on several occasions due to reflections in packaging and/or nonuniformity of the test cell. The uncertainties of the scaling factors were utilized through the weighted least sum of squares fit and was also propagated through the measurement to give a final uncertainty on the spectral irradiance responsivity. These results indicate that this hybrid spectral responsivity method presents a very viable and accurate route for irradiance spectral responsivity and short circuit current calibrations of various types of solar cells as a primary method of calibration.

8. Acknowledgements

The authors would like to thank Aarohi Vijh of Alta Devices for providing the GaAs test samples used in this study and Jeanne Houston and Howard Yoon of NIST for calibration of all reference detectors used in this work and for their advice and support. We are also grateful to Toni Litorja for the area measurements of the pinhole apertures.

9. References

1. B. H. Hamadani, J. Roller, B. Dougherty, F. Persaud, and H. W. Yoon, "Absolute spectral responsivity measurements of solar cells by a hybrid optical technique.," Appl. Opt. **52**, 5184–93 (2013).

2. J. S. Hartman and M. A. Lind, "Spectral response measurements for solar cells," Sol. Cells **7**, 147–157 (1982).

3. J. Metzdorf, "Calibration of solar cells. 1: The differential spectral responsivity method.," Appl. Opt. **26**, 1701–1708 (1987).

4. J. Metzdorf, S. Winter, and T. Wittchen, "Radiometry in photovoltaics: calibration of reference solar cells and evaluation of reference values," Metrologia **37**, 573–578 (2000).

5. "Standard test method for spectral responsivity measurements of photovoltaic devices," ASTM Stand. E1021-12 **12.02**, 502–511 (2012).

6. T. C. Larason and J. M. Houston, "Spectroradiometric detector measurements: ultraviolet, visible, and near-infrared detectors for spectral power," NIST Spec. Publ. **250**–**41**, (2008).

7. G. Xu and X. Huang, "Primary Calibration of Solar Photovoltaic Cells At the National Metrology Centre of Singapore," Energy Procedia **25**, 70–75 (2012).

8. S. Winter, T. Wittchen, and J. Metzdorf, "Primary reference cell calibration at the PTB based on an improved DSR facility," Proc. 16th Eur. Photovolt. Sol. Energy Conf. 1–4 (2000).

9. Y. He, L. Xiong, J. Zhang, H. Meng, C. Cai, B. Zhang, L. Xie, and D. Liu, "Primary calibration of solar cells based on DSR method at the National Institute of Metrology of China," Proc. SPIE **9623**, 96230S (1-5) (2015).

10. S. Winter, T. Fey, I. Kröger, D. Friedrich, K. Ladner, B. Ortel, S. Pendsa, and F. Witt, "Design, realization and uncertainty analysis of a laser-based primary calibration facility for solar cells at PTB," Meas. J. Int. Meas. Confed. **51**, 457–463 (2014).

11. J. A. Rodríguez, M. Fortes, C. Alberte, M. Vetter, and J. Andreu, "Development of a very fast spectral response measurement system for analysis of hydrogenated amorphous silicon solar cells and modules," Mater. Sci. Eng. B **178**, 94–98 (2013).

12. G. Zaid, S.-N. Park, S. Park, and D.-H. Lee, "Differential spectral responsivity measurement of photovoltaic detectors with a light-emitting-diode-based integrating sphere source.," Appl. Opt. **49**, 6772–83 (2010).

13. A. Paduthol, M. K. Juhl, and T. Trupke, "Correcting the effect of LED spectra on external quantum efficiency measurements of solar cells," IEEE J. Photovoltaics **8**, 559–564 (2018).

14. P. K. Yang, "Determining the spectral responsivity from relative measurements by using multicolor light-

emitting diodes as probing light sources," Optik (Stuttg). **126**, 3088–3092 (2015).

15. B. H. Hamadani, J. Roller, A. M. Shore, B. Dougherty, and H. W. Yoon, "Large-area irradiance-mode spectral response measurements of solar cells by a integrating sphere source," Appl. Opt. **53**, 3565–3573 (2014).

16. B. H. Hamadani, J. Roller, B. Dougherty, and H. W. Yoon, "Challenges of Irradiance-mode Spectral Response Measurements," in *40th IEEE PV Specialist Conference* (2014), pp. 1875–1878.

17. B. H. Hamadani, A. Shore, J. Roller, H. W. Yoon, and M. Campanelli, "Non-linearity measurements of solar cells with an LED-based combinatorial flux addition method," Metrologia **53**, 76–85 (2016).

18. J. R. Taylor, *An Introduction to Error Analysis*, Second Edi (University Science Books, 1982).